Experimental Measurements of Material Damping in Free Fall with Tunable Excitation

Edward F. Crawley* and David G. Mohr†
Massachusetts Institute of Technology, Cambridge, Massachusetts

An experimental method of measuring material damping of a specimen in free fall has been developed. An initially simply supported test specimen was simultaneously excited and lofted into free fall with a spring-mass launcher. The launcher could be tuned to produce varying initial stress amplitude levels in the specimens. Damping information was obtained from the transient response of the specimens while in free fall in vacuum. A dynamic model of the launch process was developed that indicates the range of frequency and initial specimen stress amplitude over which tests can be performed. To verify the facility, material damping was measured in 2024-T3 aluminum, and $[\pm 45]_{2s}$ AS1/3501-6 graphite/epoxy. Free-free frequencies ranged from 20 to 357 Hz in aluminum, and from 18 to 171 Hz in the $[\pm 45]_{2s}$ specimens. Damping values in aluminum were found to be close to theoretical values and independent of stress levels below 130 MPa (18.7 ksi). Damping ratios in the $[\pm 45]_{2s}$ graphite/epoxy specimens were found to be largely independent of stress levels below 43.8 MPa (6.35 ksi) and only slightly dependent on frequency. A small dependence of the frequency of free vibration on specimen stress amplitude was also noted.

Introduction

PASSIVE damping plays a key role in the dynamics of structural systems. Even small levels of passive damping are critical in assuring the stability of systems, especially in the presence of homogeneous unsteady aerodynamic, or closed-loop control forces. Furthermore, a knowledge of damping is essential for a complete characterization of the system dynamics.

In terrestrial applications the sources of system damping include material damping, structural damping at joints and fittings, transmission and frictional losses at support interfaces, and aeroacoustic dissipation. In space, the absence of aeroacoustic and support losses places even greater relative importance on intrinsic material and structural damping.[1,2] It thus becomes imperative to experimentally quantify the material damping in candidate materials for space structures, and the total structural damping of typical space structure geometries. The development of precise experimental techniques to measure material and structural damping under space-like conditions, and the measurement of these properties, constitute the objectives of this investigation.

A number of experimental techniques and geometries are employed to measure damping. The most common geometry is the cantilever or double cantilever arrangement, used in conjunction with the resonant dwell, half-power bandwidth, or transient decay measurement techniques.[3,4] A second common geometry is one in which the specimen vibrates in a free-free mode, suspended by wires at nodal points.

All measurement techniques necessarily influence the very quantity being measured. When measuring small levels of damping, it is especially important to minimize the influences of the measurement technique. In cantilevered test geometries, transmission and friction at the specimen-clamp interface are known to be a loss mechanism that obscures the pure material damping. To minimize these interface losses, the test specimen and mounting are often fabricated from a single larger piece of material. When testing laminated composite material, such sharply tapered specimens are often difficult or impossible to fabricate. Because of this fabrication difficulty, the free-free geometry is an obvious choice for use with laminated materials. In this geometry the specimen boundary conditions are better defined, but losses can still take place by transmission through the suspension wires.

As an alternative to suspending the specimen, it can be lofted in a free-free mode into free fall in a vacuum, eliminating all support and aerodynamic interaction.[5] Such a lofting technique is also suited to the testing of space structures, since for a short period of time a simulation of the space conditions of vacuum and zero gravity are produced in the laboratory. Although no differences are expected between material damping behavior in one and zero gravity, there is reason to expect some change in the structural damping. In a multielement jointed structure, the presence of gravity loading acting on the nonlinear joints can alter the structural damping from that measured in the absence of gravity

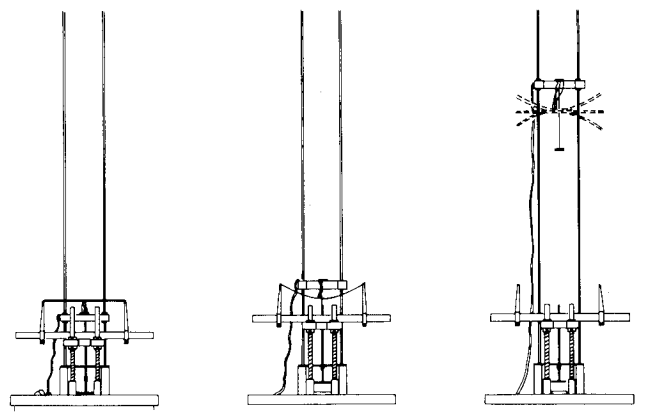

Fig. 1 Operation of the launcher/excitation mechanism, showing: a) specimen resting on supports; b) the instant of release with specimen deflected; and c) specimen in free flight, with signal wires connected to a moving terminal block.

Presented as Paper 83-0858 at the AIAA/ASME/ASCE/AHS 24th Structures, Structural Dynamics and Materials Conference, Lake Tahoe, Nev., May 2-4, 1983; received May 25, 1983; revision submitted Jan. 1984.

*Boeing Assistant Professor of Aeronautics and Astronautics, Space Systems Laboratory, Department of Aeronautics and Astronautics. Member AIAA.

†Research Assistant, Space Systems Laboratory, Department of Aeronautics and Astronautics.

loading. A preliminary assessment of such effects has been carried out at the NASA Langley Research Center.[6]

In order to gain useful parametric information about material damping from such free fall tests, the experiment must provide for independent control of specimen frequency and stress amplitude level, two of the parameters upon which material damping is expected to depend.[7] In addition, provision must be made to acquire sufficient data from the free falling test article in such a way as to not interfere with its motion.

A unique facility has been constructed at MIT to meet these objectives and measure the transient decay of a specimen while in free fall.[8] The central feature of this facility is a spring-loaded launcher located in a vacuum chamber, shown in Fig. 1. The test procedure was begun by cocking the launcher to a predetermined distance and temporarily holding it in that position with an electromagnet (Fig. 1a). An instrumented specimen was then placed on the two knife-edge supports of the launcher, and the chamber was sealed and evacuated to 1 Torr. Upon release by the electromagnet, the launcher sprung upward, accelerating the specimen and causing a deflection, as shown in Fig. 1b. After a predetermined stroke, the launcher was sharply decelerated and the specimen lofted into free flight in a free-free mode.

Details of the launch process and beginning of free flight can be seen in the stroboscopic photograph in Fig. 2. The specimen can be seen to behave essentially as a simply supported beam prior to launch, and as a free-free beam after launch. The flight time up and down the 2-m chamber was approximately 1 s. The initial stress level and rigid body velocity were controlled by adjusting the dynamics of the launch, a model of which will be presented below. The frequency of the test was varied by changing the length of the specimen.

As a verification of the facility's capability to accurately measure low levels of damping, tests were conducted on aluminum and graphite/epoxy specimens. The literature is rich in both analytic and experimental studies of material damping in both aluminum[9,10] and graphite/epoxy.[11,12] Comparison of data on aluminum is straightforward due to its homogeneous isotropic makeup. Comparison of graphite/epoxy data is more difficult due to the wide variety of fiber/resin systems in use, its anisotropic nature, and its sensitivity to the test environmental conditions. Data collected in the MIT facility will be compared with previous experiments as appropriate.

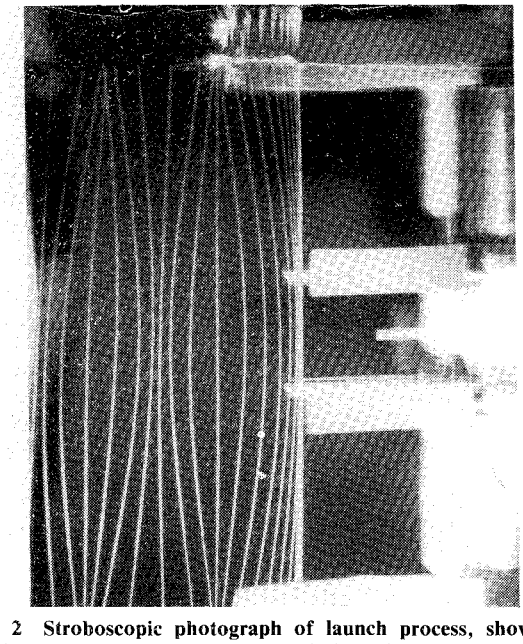

Fig. 2 Stroboscopic photograph of launch process, showing the specimen accelerated by launcher and in free flight.

Design of a Tuned Launcher

Model of Launcher Dynamics

The dynamics of the launch process establish both the rigid body velocity and the initial stress amplitude of the specimen at the instant of separation from the launcher. The initial rigid body velocity controls the height to which the specimen is lofted and therefore the time over which data can be acquired in free fall. In order to investigate these launch dynamics an analytic model of the simple lofting of an elastic beam from a spring loaded launcher was derived. This simple model provides an understanding of the launch process, as well as guidance for sizing of the launcher, and its adjustment during testing.

The specimen-launcher system is modeled as a two-degree-of-freedom system shown in Fig. 3. The launcher consists of a rigid, moving base which supports the specimen, and a compression spring. The relative displacement of the specimen with respect to the launcher base, $v(x,t)$, is approximated by a single mode

$$v(x,t) = \phi_2(x) q_2(t) \tag{1}$$

Prior to the instant of separation from the launcher, the specimen behaves as a simply supported beam. The assumed mode is therefore chosen as the first flexural mode of a simply supported beam.

$$\phi_2(x) = \sin(\pi x/\ell) \tag{2}$$

The absolute displacement of the specimen is given by

$$w(x,t) = q_1(t) + \phi_2(x) q_2(t) \tag{3}$$

where q_1 is the displacement of the launcher. If the mass of the launcher base is much greater than the mass of the specimen, the influence of the launcher on the specimen can be treated as an applied acceleration, and the governing equation of specimen motion can be given as

$$m_{22}\ddot{q}_2 + m_{22}\omega_0^2 q_2 = -m_{12}\ddot{q}_1 \tag{4}$$

where

$$m_{11} \int_0^\ell \mathrm{d}m, \quad m_{12} = \int_0^\ell \phi_2 \mathrm{d}m, \quad m_{22} = \int_0^\ell \phi_2^2 \mathrm{d}m$$

The integrals have been evaluated over the length ℓ of the beam.

Before the test, the launcher spring is precompressed by an amount A. Under these initial conditions and the assumption that the launcher base is much more massive than the specimen, the launcher displacement q_1 is given by

$$q_1(t) = -A\cos\omega_b t \tag{5}$$

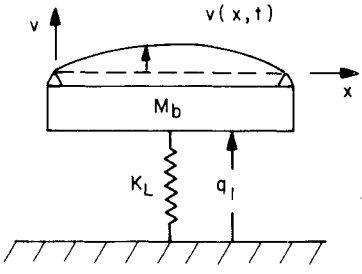

Fig. 3 Two degree-of-freedom model of specimen, launcher base (M_b) and spring (K_L).

where $\omega_b = (K_L/M_b)^{1/2}$, the natural frequency of the launcher base and spring system. Substitution for $\ddot{q}_1$ from Eq. (5) into Eq. (4) and solution for $q_2(t)$ yields

$$q_2(t) = \frac{m_{12}}{m_{22}} \frac{A\kappa^2}{(1-\kappa^2)} (\cos\omega_0 t - \cos\kappa\omega_0 t) \tag{6}$$

where $\kappa = \omega_b/\omega_0$ and $\omega_0 = \pi^2(EI/m\ell^4)^{1/2}$, the first natural frequency of a simply supported beam. As in conventional beam notation, E is the longitudinal elastic modulus, I the area moment of inertia, and m the mass per unit length.

The two parameters of interest at the instant of launch, the beam's rigid body velocity and initial stress level (peak stress), can be derived from the displacements as follows

$$q_{CG} = q_1 + q_2(m_{12}/m_{11}) \tag{7}$$

$$\sigma_{max} = \sigma\left(x = \frac{\ell}{2}, y = \frac{h}{2}\right) = -\frac{Eh}{2}\frac{\pi^2}{\ell^2} q_2 \tag{8}$$

where the maximum stress is expected at the midpoint, $x = \ell/2$, and on the surface, $y = h/2$ (h being the total thickness of the specimen).

For a given launcher and specimen, the two independent parameters necessary to specify the rigid body velocity and initial stress level are the initial spring precompression amplitude A and the instant of separation of the specimen from the launcher t_L. If the precompression A and launch time t_L are chosen such that

$$\dot{q}_{CG}(t_L) = \sqrt{2gH} \tag{9}$$

then the specimen will travel the full height H of the vacuum chamber. Equation (9) places one constraint on the choice of A and t_L. Within this constraint, and a further limitation discussed below, different combinations of A and t_L can be chosen such that different initial stress levels are produced.

Physically the launch time is enforced by adjusting the location of a hard stop, which limits the launcher stroke. When the launcher strikes the hard stop it is rapidly decelerated, lofting the specimen upward. The stroke and enforced launch time are related through Eq. (5). One further restriction on the enforced launch time t_L is that it must occur prior to the natural release time t_F, defined as the instant at which the upward force exerted by the launcher on the specimen vanishes. The natural release time is given by the first nontrivial solution of

$$\ddot{q}_{CG}(t) - g = 0 \tag{10}$$

At this natural release time the specimen would leave the launcher due to its homogeneous dynamics. The required relationship between the enforced and natural launch time is shown in Fig. 4.

In summary, for a given launcher and specimen, the two dependent variables of the launch process, the initial stress and rigid body velocity, can be prescribed within limits by properly setting the two independent variables: launcher precompression and enforced launch time. The enforced launch time is set by the stroke and must be less than the natural release time given by Eq. (10).

Launcher Design Criteria

The results of the previous section give the launch conditions for a *given* launcher and specimen, but what do they imply about the design of the launcher? From a practical point of view, a good launcher design must provide the greatest possible stress range for testing, yet not require an excessive force to precompress the launcher spring (especially if the force is exerted by hand!).

It was found that the largest stress amplitude in the free-free mode was achieved if the instant of launch coincided with the time of maximum deflection of the specimen supported on the launcher.[8] This implies that to reach the largest specimen stress amplitude, launch should occur when

$$\dot{q}_2(t_I) = 0 \tag{11}$$

and Eq. (9) is satisfied. These are referred to as the ideal launch conditions and the time at which they occur is denoted t_I. The design launch parameters were then calculated using the lesser of the ideal launch time and the quarter period of the launcher frequency.

$$\begin{aligned} t_L &= t_I & t_I &\le \pi/2\omega_b \\ &= \pi/2\omega_b & t_I &> \pi/2\omega_b \end{aligned} \tag{12}$$

This last condition assures that the compression springs are not drawn into tension, a situation which is not physically realizable.

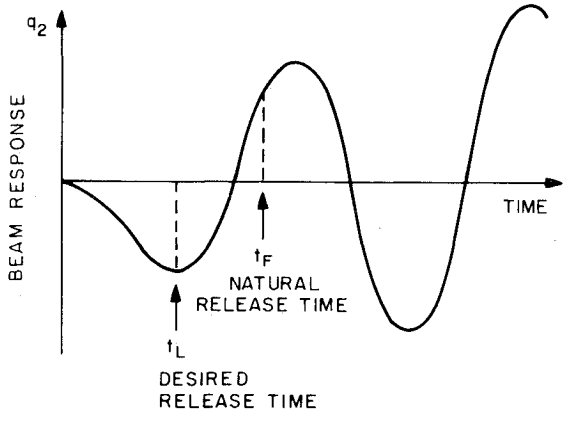

Fig. 4 Timing of launch process showing expected beam response vs time. Beam can be launched by rapidly decelerating the launcher at any time t_L prior to t_F, the natural release time.

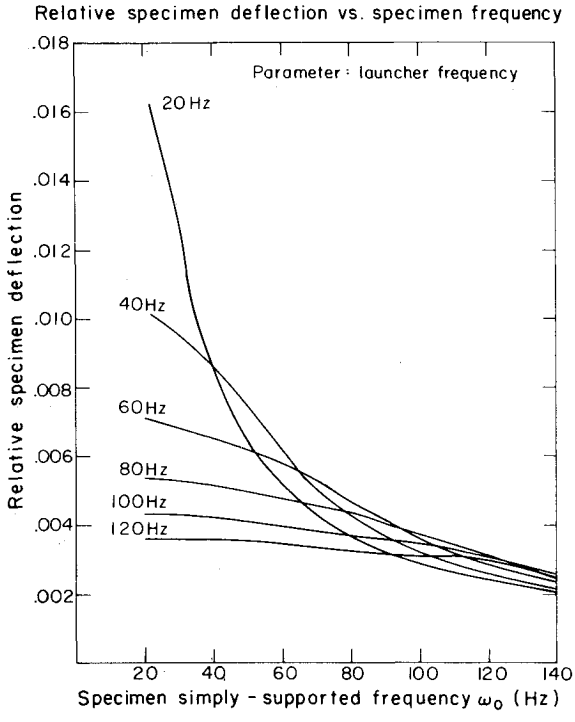

Fig. 5 Design curves for specimen deflection.

For this design launch time the relative specimen deflection for a range of launcher frequencies is given as a function of specimen frequency in Fig. 5. Examining Fig. 5, it becomes clear that a lower launcher frequency produces a larger stress level at low specimen frequencies, without a significant loss of capability at higher specimen frequencies. A low launcher frequency then is indicated, especially if one is interested in the stress-level dependence of material damping in low frequency ranges (e.g., for space structure applications).

For practicality and ease of operation, it was desired to keep the force required for launcher precompression to a minimum. The launcher compression force normalized by the launcher mass is shown in Fig. 6 for the design launch conditions given by Eq. (12). It is evident that, to minimize the force needed to cock the launcher, a low launcher frequency and low mass of the launcher base should be chosen.

Practical Launcher Implementation

The principal characteristics of the actual launcher are shown in Fig. 1. The test specimen rests on two supports, which can be moved along a horizontal tube to accommodate specimens of various lengths. The horizontal tube is attached to an aluminum frame that houses four linear bearings. The bearings ride on four case-hardened steel rods, that also stabilize the compression springs. The rods are attached to a base that can be leveled to control the trajectory of the specimen. The frequency of the launcher was chosen to be 20 Hz.

From the preceding dynamic analysis it is clear that the precompression A and launch time t_L are the variables which control the stress level and lofting height. It is therefore necessary to incorporate into the launcher mechanism a means of independently controlling these variables.

In the present launcher, the compression is adjusted by changing the length of a threaded rod, which connects the frame carrying the horizontal tube to the restraining electromagnet. Controlling t_L implies adjusting the stroke length. This is set by adjusting the location of a nut on the threaded rod that strikes a stopper plate, rapidly decelerating the launcher and lofting the specimen. These simple but effective adjustments provide very precise control over compression and stroke, and therefore allow the full range of initial stress level variation.

Table 1 Aluminum specimens (mass/unit length = 1.088 g/cm)

Specimen	Length, cm	Width, cm	Thickness, cm	First free-free frequency, Hz
1[a]	45.72	2.54	0.155	19.67
2	45.72	2.54	0.155	39.60
3	35.56	2.54	0.155	65.47
4	25.40	2.54	0.155	128.41
5	15.24	2.54	0.155	357.50

[a] Specimen 1 is specimen 2 with two 56.6 g tip masses.

Table 2 Graphite/epoxy specimens (mass/unit length = 0.421 g/cm, width = 2.51 cm, thickness = 0.104 cm)

Specimen	Length, cm	First free-free frequency, Hz	Elastic modulus, GPa
$[\pm 45]_{2s}-1$	45.72	17.95	19.6
$[\pm 45]_{2s}-2$	35.86	29.62	20.2
$[\pm 45]_{2s}-3$	25.40	54.16	20.5
$[\pm 45]_{2s}-4$	15.16	171.04	21.5

Experimental Procedure

The testing was performed inside a cylindrical plexiglass vacuum chamber 0.4 m in diameter and 2 m high. The clear cylinder walls allowed visual inspection of the lofting portion of the flight. The launcher was located at the base of the chamber, surrounded by foam rubber to cushion the impact of the specimen at the end of the test.

The specimens were instrumented with two BLH foil-type resistance strain gages, located on the top and bottom surfaces at midspan. These gages were connected via four 39-gage copper wires 0.5 m long, leading to a terminal strip that was attached to an aluminum block. During the test, the aluminum block with the terminal strip rides on linear bearings along two guide rods which span the height of the vacuum chamber, and are visible in the background in Fig. 1c. Since the block is launched at the same time and with the same rigid body velocity as the specimen, it will follow the same vertical trajectory in time. The short thin wires connected to the specimen therefore remain slightly slack and exert no significant influence on the specimen during its flight. A completely nonintrusive laser Doppler velocimeter was also developed to measure the velocity response of the specimen in free fall. However, due to the difficulty of tracking the specimen, the velocimeter never produced data of sufficiently high signal to noise ratio to warrant its incorporation into the test facility.

As can be seen in Fig. 1c, the terminal block drags with it a heavier shielded cable, through which the strain gage signal is passed to an instrumentation amplifier. During typical tests, the component of strain associated with the specimen's third bending mode was observed to have approximately one tenth the amplitude of that due to the first mode. To separate these two modal responses, the analog data were filtered with an 8-pole lowpass Butterworth filter. The passband of the filter was set logarithmically halfway between the first and third natural frequencies. Both filtered and unfiltered data were digitized.

The tests were conducted by first presetting the launcher compression and stroke, energizing the electromagnets, and cocking the launcher and terminal block. The specimen was placed on the supports, the chamber evacuated to 1 Torr, and the test was performed. Each specimen was tested at three progressively higher stress levels and each stress level test was repeated three times.

Specimen natural frequencies and critical damping ratios were determined by performing a least-squares fit of an exponentially decaying sinusoid to the strain gage data. From this least-squares fit, the damping ratio and frequency of the specimen were determined. A damping ratio determined in this way is approximately equivalent to one determined by a log-decrement method. The distinction is that the least-squares fit uses all of the data points rather than just the peak points as in the log-decrement method.

An initial comparison of fit results obtained from filtered and unfiltered data showed no difference in measured damping ratio for the fundamental mode. Subsequent analysis considered only the filtered data. To allow more detailed resolution of damping ratio as a function of stress level, each test was divided into three data windows of approximately 300 ms duration. A fit was made to each window and the values of natural frequency and damping ratio were averaged for windows of similar frequency and stress level (defined as the mean stress during the window). Stress levels were calculated from measured strain levels and Young's modulus.

Material Damping Results

In order to verify the experimental procedure, a study was first performed on aluminum. Specimens were fabricated from 0.165 cm (0.065 in.) thick 2024-T3 aluminum sheet to the dimensions listed in Table 1. All surfaces were sanded to relieve machining stresses and surface scratches.

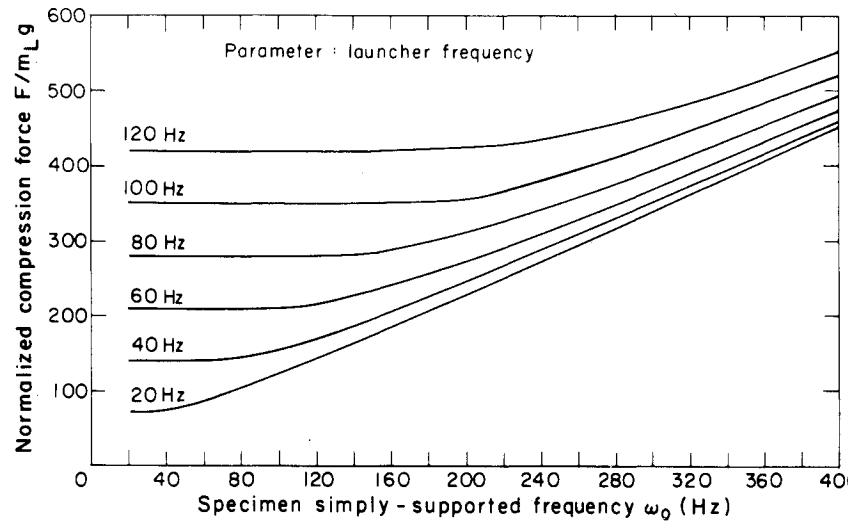

Fig. 6 Design curves for normalized launcher compressive force.

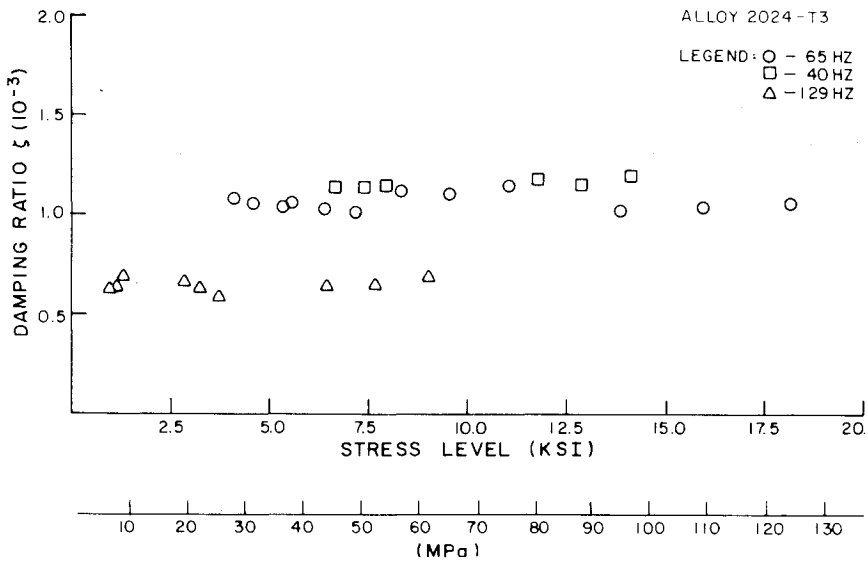

Fig. 7 Damping ratio vs stress level in aluminum.

The aluminum specimens were tested at room temperature and at stress levels from 3.5 to 130 MPa (0.5 to 18.7 ksi). Damping forces for the three intermediate frequencies tested were plotted against measured stress levels, as shown in Fig. 7. The damping ratio shows no significant dependence on stress level, which is in good agreement with previous studies.[9]

The plot of damping ratio vs frequency in Fig. 8 shows an interesting trend. Above the maximum, the results show excellent agreement with theory[13] and previous experiments.[5,9,10] However, unlike the theoretical curve and the results of Ref. 10, the damping ratio from the current data does not substantiate a decline in damping for the one frequency below the relaxation frequency ω_n, which is derived from the thermoelastic heating model of Zener.[13]

$$\omega_n = (\pi^2 k/h^2 c) \tag{13}$$

where k is the material thermal conductivity, c the specific heat per unit volume, and h the specimen thickness.

An interesting demonstration of the current technique's precision can be obtained if measured frequency of a given specimen is plotted against stress level at which the measurement was made. Figure 9 clearly shows the decrease of effective Young's modulus with increasing specimen peak stress amplitude. The trend of decreasing frequency with increasing stress was noted for the lower frequency aluminum specimens. One possible explanation of this phenomenon is the presence of slight plasticity effects at higher stress levels, which would cause softening. However, note that the modulus begins to decrease even at extremely low stress levels.

Although a formal error analysis of the data is difficult due to the least-squares fitting procedure, some indication of accuracy can be gained by observing the consistency and precision of the results shown for damping in Fig. 7 and for frequency in Fig. 9. Variations in damping of the order of 1 part/10,000 of critical damping are consistently measured. Likewise, variations of smaller than 1 part/1,000 in frequency are indicated in Fig. 9. Different least-squares fits to the same data window indicate consistent measurement of frequency to 3 parts/10,000.

As an initial effort to characterize material damping in composite materials, a series of measurements were made on $[\pm 45]_{2s}$ graphite/epoxy specimens. The graphite/epoxy specimens were fabricated from AS1/3501-6 prepreg tape. The specimens were cured according to manufacturer's specifications.[8] Tests were initially performed using a 45.7 cm (18 in.) specimen. In order to reduce scatter due to material property variation, successively shorter specimens were obtained by reducing the length of this 45.7 cm (18 in.) specimen. Specimen dimensions and frequencies are listed in Table 2. Testing was performed at room temperature and using laminates of low moisture content.

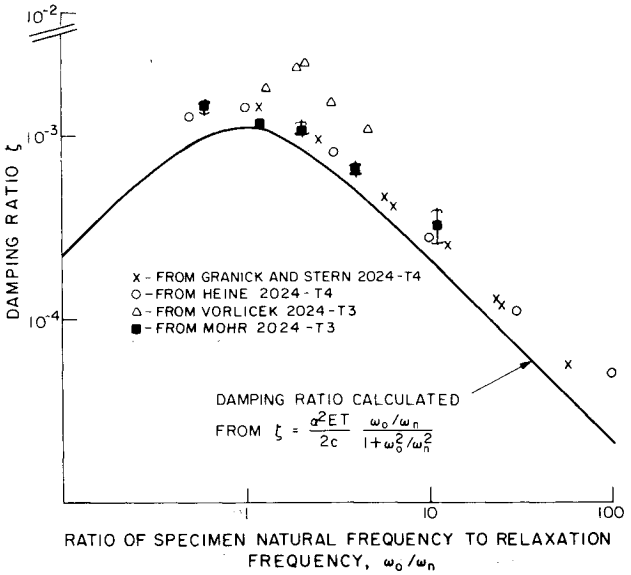

Fig. 8 Damping ratio vs ω_0/ω_n in aluminum.

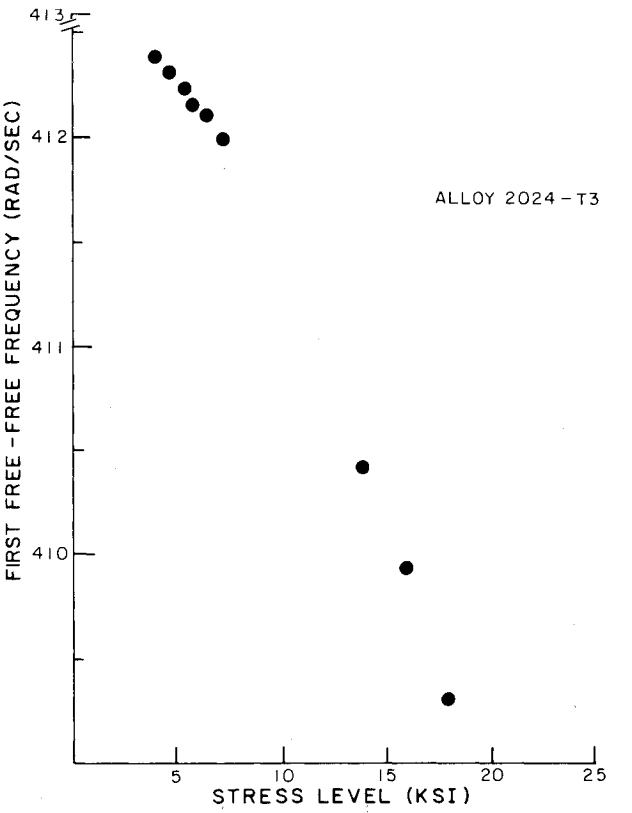

Fig. 9 Measured free-free frequency vs stress in aluminum.

The $[\pm 45]_{2s}$ laminates were tested at stress levels from 1.4 to 43.8 MPa (0.2 to 6.35 ksi). A plot of damping ratio vs stress level (Fig. 10) shows damping to be perhaps only slightly dependent on stress level. In Fig. 11, a slight increase in damping with frequency can be seen.

The average damping value and trend of increasing damping with frequency agree quite well with those of Ref. 12, in which tests were carried out on $[\pm 45]_{3s}$ laminates of Narmco 5208/T300 graphite/epoxy, tested at 25°C and dry conditions.

Values for the longitudinal elastic moduli of the $[\pm 45]_{2s}$ graphite/epoxy specimens as calculated from the measured frequency are presented in Table 2. In the $[\pm 45]_{2s}$ laminates the averaged measured longitudinal modulus increases slightly with increasing frequency, again in agreement with

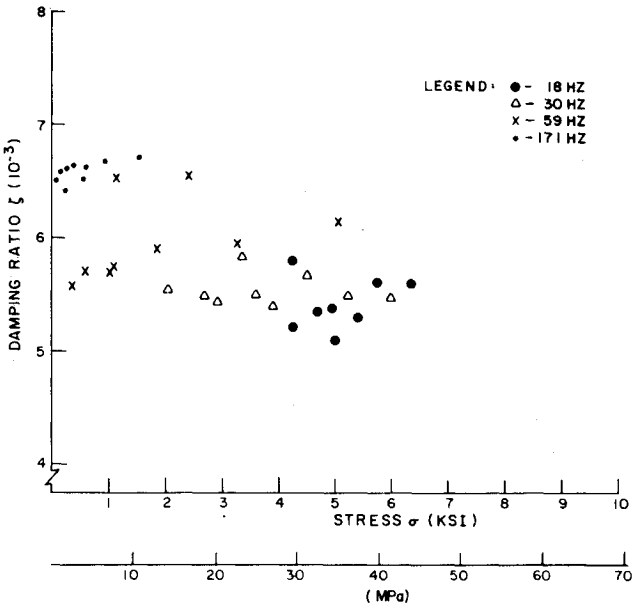

Fig. 10 Damping ratio vs stress level in $G/E\,[\pm 45]_{2s}$.

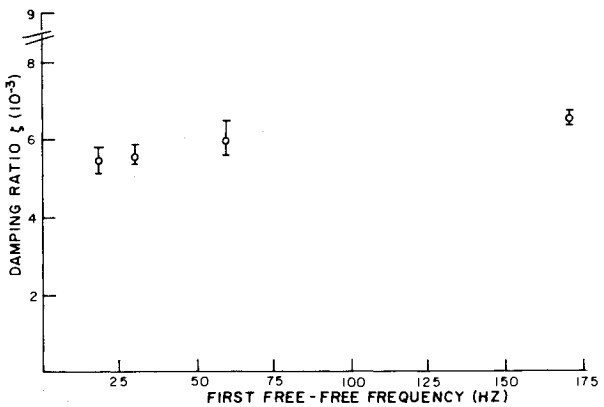

Fig. 11 Damping ratio vs frequency in $G/E\,[\pm 45]_{2s}$.

Ref. 12. Like the aluminum specimens, a slight variation in specimen frequency with stress level was also noted.

Conclusions

The measurement of material damping during transient decay in free fall in a vacuum has been shown to be a useful and precise experimental technique. The technique has as its principal advantage the elimination of virtually all support interference. Gravity loading on the structure also is effectively eliminated, a requirement which is potentially important in future testing of structural damping in space structures. By incorporation of a tuneable spring cocked launcher which simultaneously excites and lofts the specimen, independent control of stress level and frequency are achieved. The principal disadvantage of the technique is that it is more elaborate and time consuming than traditional test methods. Although no formal error analysis can be performed, the precision and constancy of measurements indicated sensitivity on the order of 1×10^{-4} of critical damping and 3×10^{-4} in frequency.

In the study of 2024-T3 aluminum it was confirmed that the material damping is independent of stress level below 130 MPa (18.7 ksi) and follows the theoretical values of Zener[13] closely for frequencies above the relaxation frequency.

Material damping in graphite/epoxy $[\pm 45]_{2s}$ was found to increase only slightly with both increasing stress level and frequency. Damping ratios ranged from 0.5 to 0.66% of critical damping in a frequency range of 18-171 Hz and a stress level range of 1.4-43.8 MPa (0.2-6.35 ksi).

A weak but constant dependence of natural frequency with stress level was found in the aluminum. At low frequency, the observed natural frequency decreased consistently with stress amplitude level.

Acknowledgments

The authors wish to acknowledge the National Aeronautics and Space Administration for their support under NASA Grant NAGW-21, with Mr. Samuel Venneri as technical monitor, and the support of the Aerospace Corporation, with Mr. James Moore and Dr. Rudolph Meyer as monitors. The authors wish to further acknowledge Prof. James W. Mar for his advice and support of this and many other projects in the MIT Space Systems Lab.

References

[1]Ashley, H., "On Passive Damping Mechanisms in Large Space Structures," AIAA Paper 82-0639, April 1982.

[2]Crawley, E. F., Sarver, G. L., and Mohr, D. G., "Experimental Measurement of Passive Material and Structural Damping for Flexible Space Structures," IAF Paper 82-380, Sept. 1982.

[3]Lazan, B. J. and Goodman, L. E., "Material and Interface Damping," *Shock and Vibration Handbook*, Vol. 2, edited by E. M. Harris, McGraw-Hill Book Co., New York, 1961, Chap. 36.

[4]Bert, C. W., "Material Damping: An Introductory Review of Mathematical Models, Measures, and Experimental Techniques," *Journal of Sound and Vibration*, Vol. 29, No. 2, 1973, pp. 129-153.

[5]Vorlicek, P. L., "Material Damping of Aluminum and Graphite/Epoxy in a Simulated Zero-Gravity Environment," M.I.T., Cambridge, Mass., Space Systems Laboratory Rept. 13-81, Jan 1981.

[6]Herr, R. W. and Horner, G. C., "Development Test of a 36-Element Tetrahedral Truss Module," *Large Space Systems Technology-1980*, Vol. II, NASA CP 2168, Second Annual Technical Review, Nov. 1980.

[7]Lazan, J., *Damping of Materials and Members in Structural Mechanics*, Pergamon Press, Oxford, 1968.

[8]Mohr, G. D. and Crawley, E. F., "Experimental Measurements of Material Damping of Aluminum and Graphite/Epoxy in Free Fall with Tuneable Excitation," M.I.T., Cambridge, Mass., Space Systems Laboratory Rept. 11-82, June 1982.

[9]Granick, N. and Stern, J. E., "Material Damping of Aluminum by a Resonant-Dwell Technique," NASA TN D – 2893, Aug. 1965.

[10]Heine, J. C., "The Stress and Frequency Dependence of Material Damping in Some Engineering Alloys," Ph.D. Thesis, M.I.T., Cambridge, Mass., June 1966.

[11]Bert, C. W., "Composite Materials: A Survey of the Damping Capacity of Fiber-Reinforced Composites," *Damping Applications for Vibration Control*, AMD Vol. 38, edited by P. J. Torwik, ASME, Nov. 1980, pp. 53-63.

[12]Putter, S., Buchanan, D. L., and Rehfield, L. W., "Influence of Frequency and Environmental Conditions on Dynamic Behavior of Graphite/Epoxy Composites," *Composite Materials: Testing and Design (Sixth Conference)*, ASTM STP 787, edited by I. M. Daniel, ASTM, 1982, pp. 414-424.

[13]Zener, C. M., *Elasticity and Anelasticity of Metals*, University of Chicago Press, Chicago, 1948.